

**FINAL REPORT ON THE MODIS NEAR-IR WATER VAPOR
ALGORITHM AND CIRRUS CLOUD REFLECTANCE ALGORITHM**

BO-CAI GAO

(FEBRUARY 2004)

Remote Sensing Division, Code 7232, Naval Research Laboratory
4555 Overlook Avenue, SW, Washington, DC 20375 USA

TABLE OF CONTENTS

1. Introduction.....	3
2. The Status of MODIS Near-IR Water Vapor Algorithm	3
3. The Status of MODIS Cirrus Reflectance Algorithm.....	9
4. Lessons Learned	14
5. References.....	16
6. Publications	17

1. INTRODUCTION

With financial support from the NASA MODIS Project Office during the past decade, we have successfully developed two operational algorithms, the *near-IR water vapor algorithm* and the *cirrus reflectance algorithm*, for processing multi-channel imaging data acquired with both the Terra and Aqua MODIS instruments. We have obtained very good water vapor retrievals over global land surfaces and over oceanic areas with Sun glint. We have also obtained excellent high cloud reflectances (mainly cirrus cloud images) over the globe during the daytime using the special 1.375- μm cirrus-detecting channel on MODIS. Here we would like to give a summary on the current status of both algorithms. We would also like to report that many MODIS' land, ocean and atmospheric data products are still contaminated by thin cirrus absorption and scattering effects. Such effects need to be removed in order to obtain the high quality MODIS products for climate studies.

2. THE STATUS OF MODIS NEAR-IR WATER VAPOR ALGORITHM

2.1. Instrument and Retrieving Technique. At present, two Moderate Resolution Imaging SpectroRadiometer (MODIS) instruments (Salomonson et al., 1989; King et al., 1992; Asrar and Greenstone, 1995) on board the NASA Terra and Aqua Spacecraft platforms are operational for global remote sensing of the land, ocean and atmosphere. MODIS has 36 channels covering the spectral region between 0.4 and 15 μm . Five near-IR channels in the 0.8 – 1.3 μm spectral region are useful for remote sensing of water vapor. The positions and widths of these channels from the original MODIS design specifications are given in Table 1. The implementation of the two water vapor channels centered at 0.905 and 0.940 μm was largely based on the work of Gao and Goetz (1990) and Kaufman and Gao (1992) with water vapor retrievals from high spatial resolution hyperspectral imaging data collected by the Airborne Visible Infrared Imaging Spectrometer (AVIRIS) (Vane et al., 1993; Green et al., 1998) from a NASA ER-2 aircraft at an altitude of 20 km.

The positions and widths of these channels together with two atmospheric water vapor transmittance spectra for the Tropical and Sub-Arctic Winter Models (Kneizys et al., 1988) are also shown in Figure 1a. The atmospheric “window” channels at 0.865 and 1.24 μm are designed for remote sensing of vegetation and clouds. The channels at 0.936, 0.940, and 0.905 μm are water vapor absorption channels with decreasing absorption coefficients. We show in Figure 1b examples of simulated transmittance ratios of 2-channels, absorption channel/window channel,

as a function of water vapor amount in the Sun-surface-sensor path. The strong absorption channel at 0.936 μm is most useful for dry conditions, while the weak absorption channel at 0.905 μm is most useful for very humid conditions, or low solar elevation.

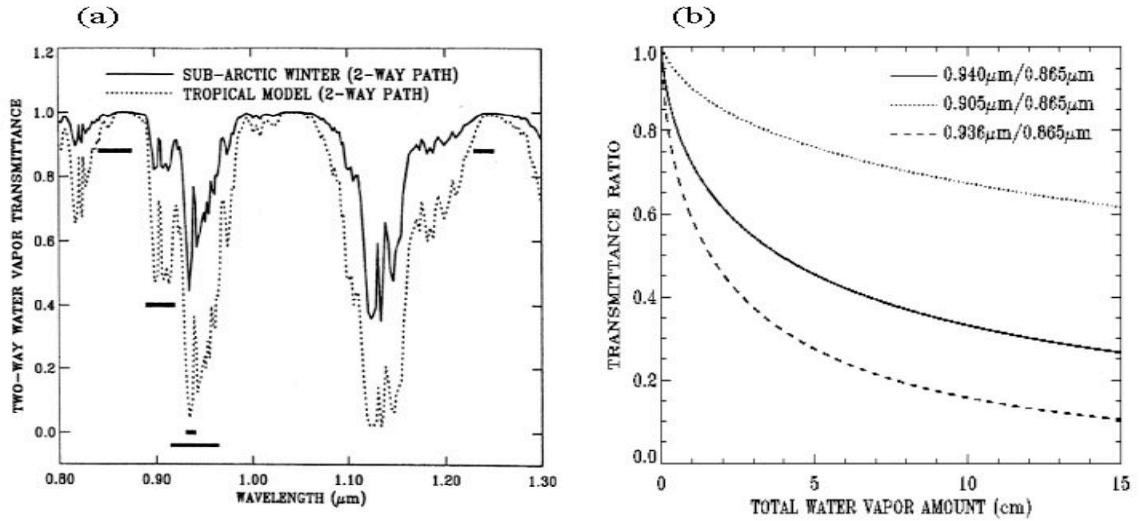


Fig. 1. (a) - Positions and widths of five MODIS near-IR channels marked in thick horizontal bars, and 2-way atmospheric water vapor transmittance spectra for the tropical and sub-arctic winter models in LOWTRAN-7 with a solar zenith angle of 45 degrees and a nadir-looking geometry; and (b) - Examples of simulated transmittance ratios of 2-channels (absorption channel / window channel) as a function of total water vapor amount in the Sun-surface-sensor path.

Table 1: Positions and widths of five MODIS near-IR channels used in water vapor retrievals.

MODIS Channel #	Position (μm)	Width (μm)
2	0.865	0.040
5	1.240	0.020
17	0.905	0.030
18	0.936	0.010
19	0.940	0.050

The near-IR water vapor algorithm relies on observations of water vapor attenuation of solar radiation reflected by the bottom surface. Techniques employing ratios of water vapor absorbing channels centered near 0.905, 0.936, and 0.940 μm with atmospheric window channels at 0.865 and 1.24 μm are used. The ratios partially remove the effects of variation of surface reflectance with wavelengths and result in the atmospheric water vapor transmittances. The column water vapor amounts are derived from the transmittances based on theoretical

calculations and the use of look-up table procedures. The lookup tables were pre-calculated using a line-by-line atmospheric transmittance code and the HITRAN2000 spectroscopic database (Rothman et al., 1998). The daily ‘pixel-based’ near-IR water vapor product, which is a standard MODIS Level 2 data product, at the 1-km spatial resolution of the MODIS instrument, and the daily, 8-day, and monthly near-IR water vapor products, which are standard MODIS Level 3 products, at a 1° by 1° latitude-longitude grid globally are now routinely produced at a NASA computing facility.

2.2. Sample Level 2 Water Vapor Images from Terra MODIS. We show in Figure 2 an example of water vapor retrieval over the Eastern United States from one set of Terra MODIS L1B data acquired at 1655 UTC on April 19, 2000. The left panel shows a false color image processed from the MODIS channels centered at 0.645 μm (red), 0.86 μm (false green), and 0.47 μm (blue). The upper part of the scene is covered by thick clouds. The lower part of the scene looks fairly clear. The right panel shows the column water vapor image. The huge “red” areas are affected by moisture coming from the Gulf of Mexico. East of the “red” areas, the “blue” areas are covered by dry air from Canada. The eastern portions of the scene are affected by the moisture originating from the Atlantic Ocean. This water vapor image demonstrated that the spatial distribution of water vapor can be mapped out quite well with MODIS near-IR channels.

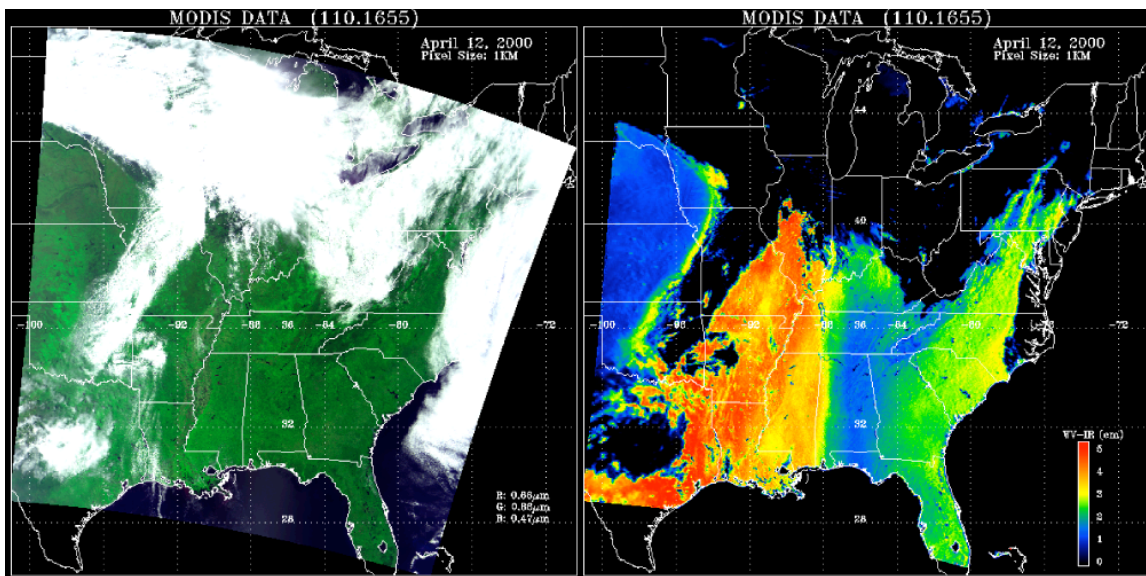


Fig. 2. An example of water vapor retrievals over the Eastern United States. See text for detailed descriptions.

We show in Figure 3 another example of water vapor retrievals from the Terra MODIS near-IR channels. The left panel shows a false color image processed from a data set acquired at 0530 UTC on April 30, 2002. The lower part of the scene covers a major portion of the Indian Continent. The upper part of the scene covers the Himalayan Mountains. The right panel shows

the column water vapor image derived from the MODIS data. Over the high elevation Himalayan mountain regions, the water vapor amounts are quite small (< 1 cm). Over the low elevation Indian Continent, the water vapor amounts are significantly greater. The high elevation of the Himalayas block the northward movement of water vapor originating from the Bay of Bengal in the lower right portion of the scene, and force the water vapor to remain over the Indian Continent.

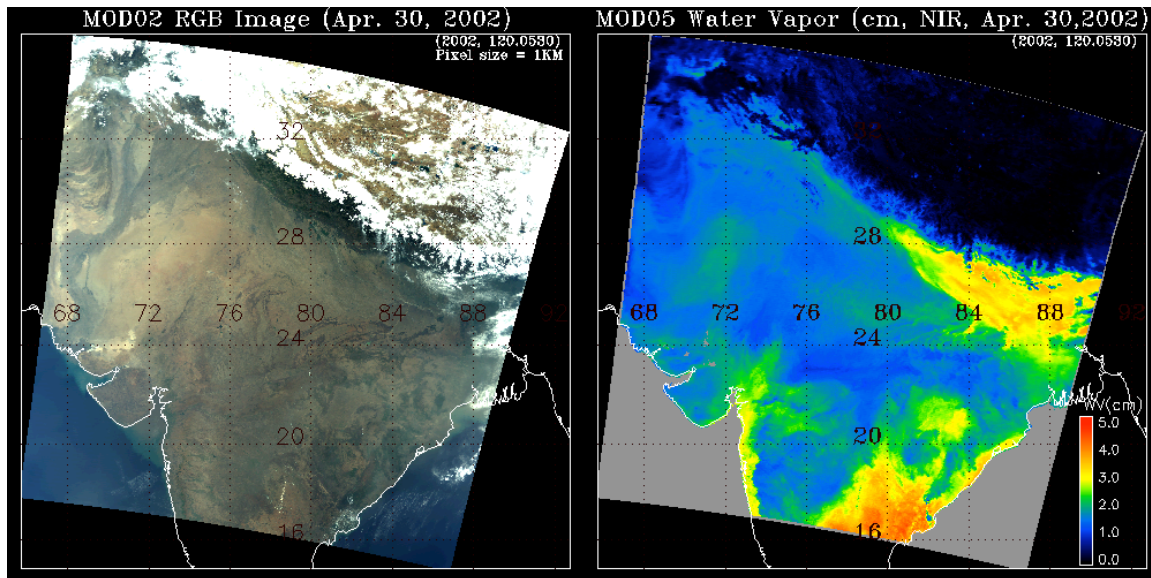


Fig. 3. An example of water vapor retrieval over the Tibetan Plateau and the Indian Continent.

2.3. Sample Level 2 Water Vapor Images from Aqua MODIS. Figure 4 shows an example of water vapor derivations from the Aqua MODIS data. In Fig. 4a we show a false color image of

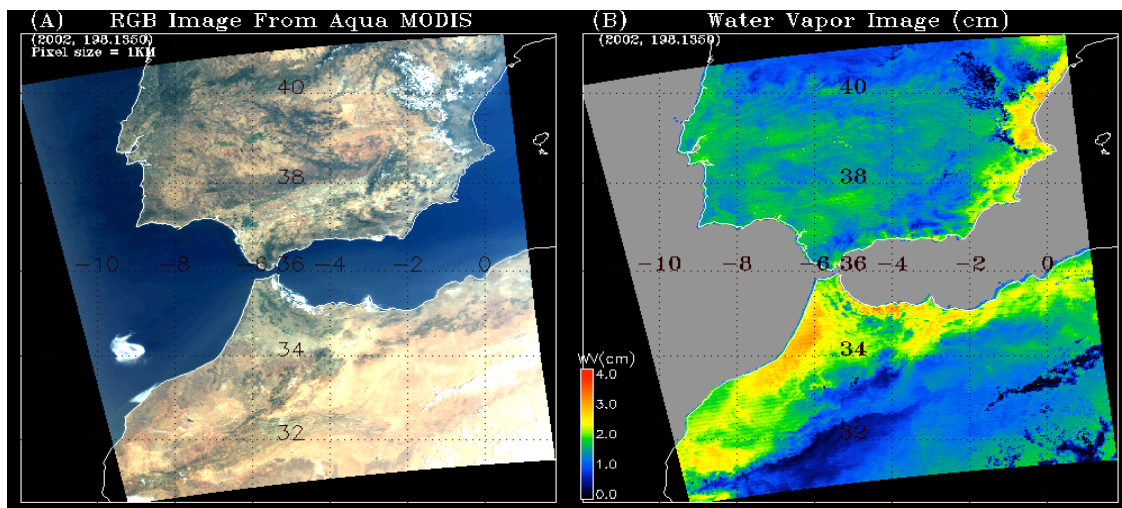


Fig. 4. An RGB image and a near-IR water vapor image obtained from AQUA MODIS measurements over Spain and Morocco.

the scene. The top part of the scene covers major portions of Spain and Portugal. The bottom part covers parts of Morocco and Algeria. Atlantic Ocean is seen in the left part of the image. The Mediterranean Sea is seen in the right part of the image. The Aqua MODIS data were acquired on July 17, 2002 at UTC 1350. In Fig. 4b we show the column water vapor image derived from the Aqua MODIS data set. The areas over land and close to the land-water boundaries have higher concentrations of water vapor. The desert areas in the bottom right portions of the scene have far less water vapor than the coastal areas. It is quite easy to see the dramatic spatial variations of water vapor in this image.

In Figure 5 we show another example of Aqua MODIS water vapor retrievals over the northern part of Africa Continent. Nile Delta is located in the middle right portion of the scene. The coast of Libya is in the center of the image. The water vapor values over land areas close to the Mediterranean Sea are significantly greater than those over the interior desert areas.

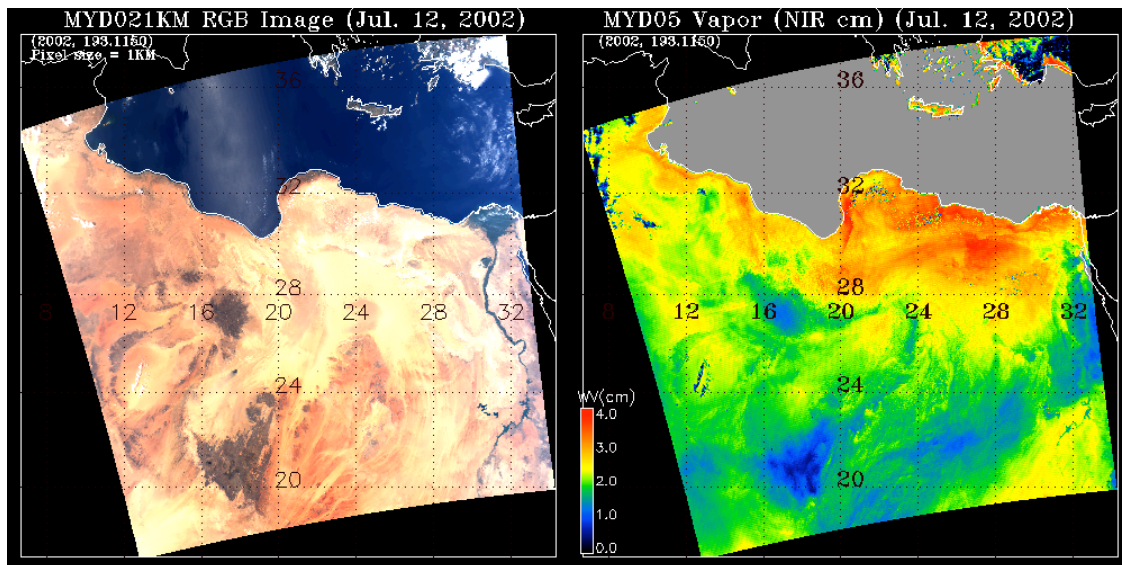


Fig. 5. An RGB image and a near-IR water vapor image obtained from AQUA MODIS measurements over northern part of the Africa Continent.

2.4. Sample Level 3 Monthly-Mean Global Water Vapor Images from Terra MODIS.

Figure 6a is a global water vapor image for January of 2001. During this northern hemisphere winter month, the water vapor amounts over most parts of North America, Europe, Asia, and northern part of the Africa Continent are quite small (< 2 cm). Only the southern parts of Indian Continent and Indo-China have relatively higher moisture contents with column water vapor amounts in the range of 3 – 4.5 cm. Brazil, the southern part of African Continent, and Australia have high moisture contents. Figure 6b is a global water vapor image for July of 2001. The northern hemisphere becomes more moist in comparison with the January image. The Indian Continent, Indo-China, and eastern part of China are now saturated with water vapor. The central

U.S. is also quite moist due to water vapor transported north from the Gulf of Mexico. The southern part of South America, southern part of the African Continent, and Australia are dry during their winter season. The high elevation areas, such as those of the Rocky Mountains in North America, the Andes Mountains in South America, the Himalayas in Asia, and the Sahara desert areas in northern Africa have low moisture contents in both the July and January images. The water vapor images in Figs. 6a and 6b show the utility of the level 3 monthly-mean near-IR water vapor images for the studies of seasonal variations of water vapor on a global scale.

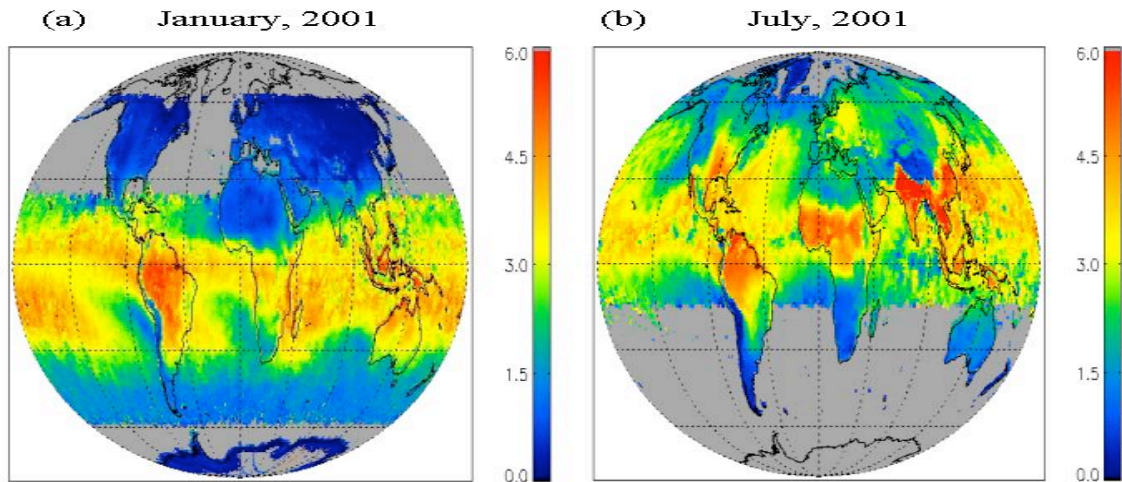


Fig. 6. Monthly-mean global Level 3 water vapor images for January 2001 (a) and July 2001 (b). The color scale on the right gives the total precipitable water vapor in cm.

2.5. Validations. We have made extensive analysis of the Level 2 and Level 3 near-IR water vapor images in order to make sure that no gross mistakes are present in our products. Other researchers at NASA Goddard and at NASA Langley have also conducted independent validation-related studies. In order to gain confidence in the accuracy of our near-IR water vapor products, we have compared the MODIS near-IR water vapor values with those measured with a ground-based upward-looking microwave radiometer located at a site in the Southern Great Plains in Oklahoma for a time period between November 2000 and December 2001. The microwave radiometer measurements were sponsored by the Department of Energy's Atmospheric Radiation Measurement Program and the data were released for public use. Figure 7 shows a scatter plot between the water vapor values measured with the microwave radiometer and the MODIS near-IR water vapor values measured on clear days. The regression analysis of the two data sets gives a slope of 0.93. Overall, the water vapor values from MODIS and from microwave radiometer measurements agree quite well with differences typically in the range between 5 and 10%. This is excellent agreement given the differences in methodology between the two measurements.

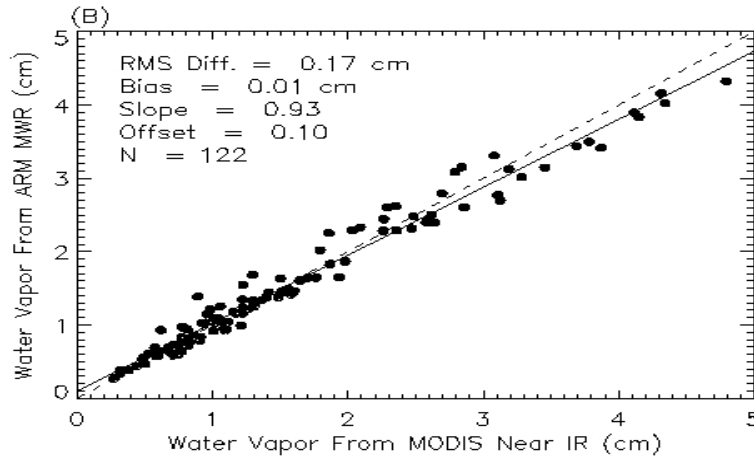


Fig. 7. A scatter plot between the water vapor values measured with a ground-based upward-looking microwave radiometer at a site in the Southern Great Plains in Oklahoma and those retrieved from images of MODIS near-IR channels for a time period between November 2000 and December 2001.

3. THE STATUS OF MODIS CIRRUS REFLECTANCE ALGORITHM

3.1. The 1.375- μm Channel for Cirrus Detections. MODIS has a near-IR channel centered at 1.375- μm with a width of 30 nm for remote sensing of cirrus clouds from space. The implementation of this channel on MODIS was largely based on our previous analysis of hyperspectral imaging data collected using the NASA JPL AVIRIS instrument with over 200 10-nm channels from an ER-2 aircraft at 20 km altitude. The mechanism for the detection of cirrus clouds using narrow channels near the center of the strong 1.375- μm water vapor band was first developed by B.-C. Gao and reported in Gao et al. (1993). Cirrus clouds are typically located in the upper troposphere and lower stratosphere. The amount of water vapor above cirrus clouds is usually 1% - 10% of the total amount of water vapor from ground to space. AVIRIS channels near 1.375 μm receive little radiance resulting from scattering of solar radiation by the surface and low-level clouds because the solar radiation is mostly absorbed by water vapor in the lower atmosphere. When cirrus clouds are present, these channels receive large amounts of solar radiance scattered and reflected by ice particles in cirrus clouds. An example of this method of cirrus detection is presented in Figure 8, which shows three AVIRIS images for channels at 0.56, 1.25, and 1.37 μm over Coffeyville, Kansas. The 1.37- μm image shows only the upper level cirrus clouds. The surface features seen in the 0.56- and 1.25- μm images have disappeared completely in the 1.37- μm image. Based on observations from the AVIRIS data, Gao and Kaufman (1995) proposed to put a special 1.375- μm cirrus detecting channel on MODIS. With

strong support from the MODIS Science Team and NASA Goddard management, the proposed channel was implemented on both the Terra and Aqua MODIS instruments.

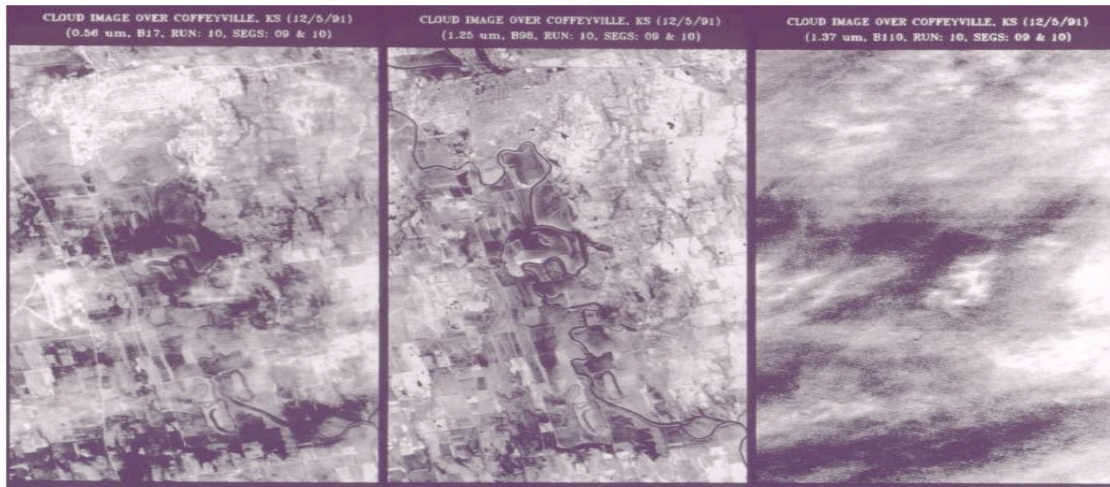


Fig. 8. Examples of AVIRIS images acquired over Coffeyville in southeastern Kansas on Dec. 5, 1991. Both the 0.56- μm and 1.25- μm images show surface features, while the 1.37- μm image shows only upper level cirrus clouds.

In order to illustrate cirrus reflectance properties, we show in Figure 9 two AVIRIS spectra (in reflectance units) acquired over areas covered by thick and thin cirrus clouds, respectively, over Monterey Bay, California. For each spectrum, the reflectances of ice particles in the 0.45 - 1.0 μm spectral region are nearly constant with wavelength, because ice particles are much larger than the wavelength and non-absorbing in this spectral region. The larger apparent reflectances in the 0.45 - 0.6 μm region are due to Rayleigh scattering. Past 1.0 μm one finds several ice absorption bands, for example those centered near 1.5 and 2.0 μm . Weak ice absorptions occur near 1.24 μm and 1.375 μm ; the imaginary parts of the ice refractive index are about the same at both wavelengths. The measured reflectances at 1.375 μm are smaller than those in the 0.4–1.0 μm region mainly because of absorption by water vapor above and within the cirrus clouds. These upper-level water vapor absorption effects need to be accounted for in order to use the 1.375- μm channel for quantitative removal of cirrus effects in other channels.

We have developed an empirical technique (Gao et al., 2002) using scatter plots of 1.375- μm apparent reflectances versus 0.66- μm apparent reflectances, as illustrated in Figure 10, to estimate the upper level water vapor transmittances from MODIS data. The slopes defined by the points in the upper left portions of the scatter plots are the desired transmittances. The cirrus reflectances in the 0.4 – 1.0 μm region are equal to the 1.375- μm apparent reflectances divided by the transmittances. The daily ‘pixel-based’ cirrus reflectance product, which is a standard MODIS Level 2 data product, at the 1-km spatial resolution of the MODIS instrument, and the daily, 8-day, and monthly cirrus reflectance products, which are standard MODIS Level 3

products, at a 1° by 1° latitude-longitude grid globally are operationally produced at a NASA computing facility.

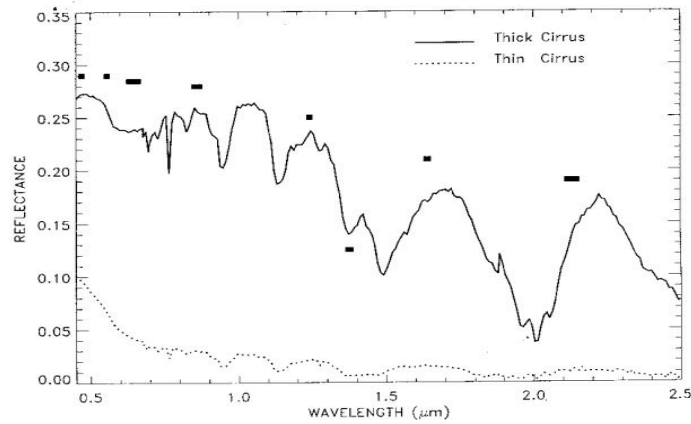


Fig. 9. Examples of AVIRIS spectra over thick and thin cirrus clouds. MODIS channels are shown as short thick bars.

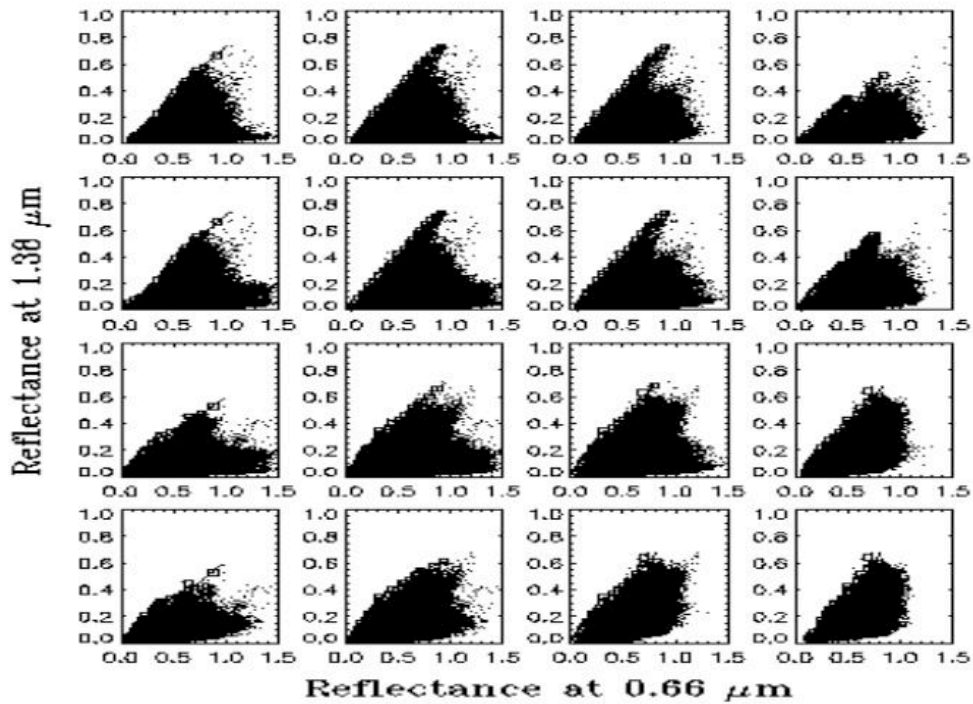


Fig. 10. Examples of scatter-plots of 1.375- μm reflectance versus 0.66- μm reflectance for 16 segments within a MODIS scene.

3.2. Sample Level 2 MODIS Cirrus Images. The left panel in Figure 11 shows a false color image (R: 0.66; G: 0.86; B: 0.46 μm) for a MODIS scene over the western part of the United States and Mexico. Many surface features, such as the bright snow over Rocky Mountains, are

seen quite well. The right panel shows the 1.375- μm channel image. Cirrus clouds, and possibly aircraft contrails embedded in natural cirrus, are easily seen in this image. Surface features, such as the land water boundary in the lower left of the image, are difficult to see. This figure demonstrates that the 1.375- μm MODIS channel is very effective for cirrus detection.

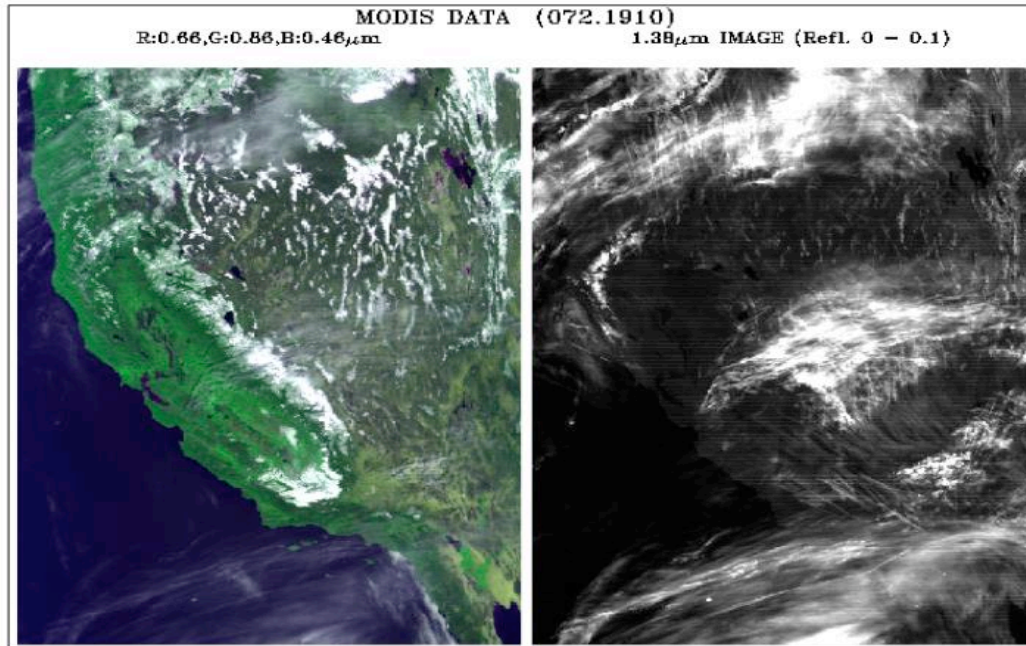


Fig. 11. A false color image (left panel) and a 1.375- μm image (right panel) processed from one set of MODIS data acquired on April 19, 2000.

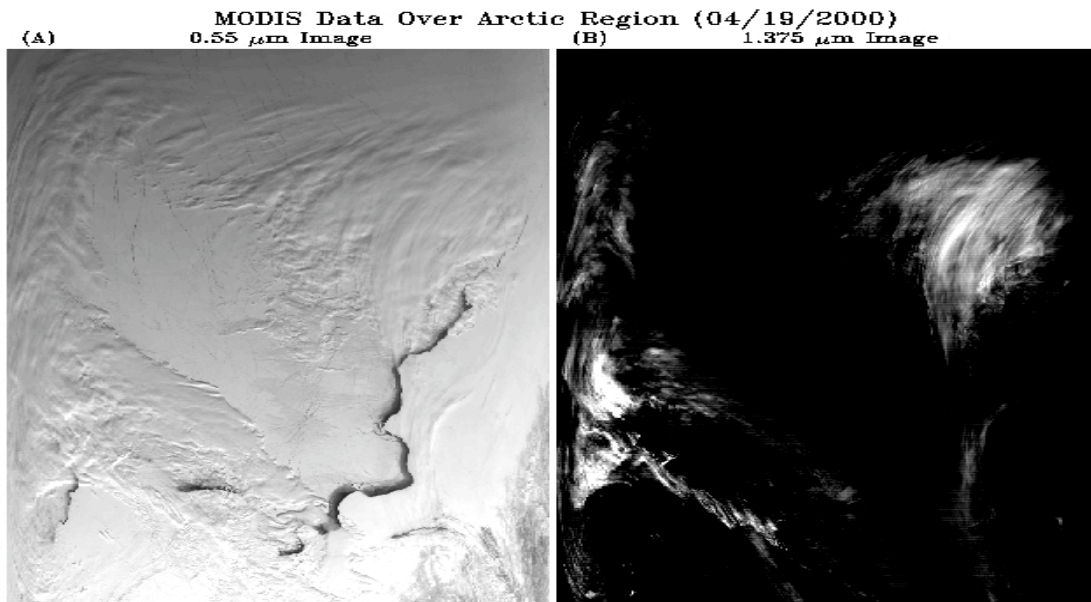


Fig. 12. The MODIS 0.55- μm channel image (a) and the 1.375- μm channel image (b) acquired over the Arctic region on April 19, 2000 at UTC 0510.

Through viewing large number of Level 2 images at the 1-km spatial resolution of the MODIS instrument, we have found that high clouds in the polar region can be observed routinely with the 1.375- μm channel during the daytime. Figure 12a shows a 0.55- μm channel image acquired over the Arctic region on April 19, 2000 at UTC 0510. The image covered parts of Russia and areas north of Russia. Surface features are obvious in this image, while cloud features are difficult to see. Figure 12b shows the 1.375- μm channel image acquired over the same areas. Cloud features are seen quite well in this image, while surface features are hardly seen. This image clearly demonstrates the capability of detecting clouds over the Arctic region using the 1.375- μm MODIS channel.

3.3. An example of cirrus path radiance removal. One of the purposes for retrieving cirrus reflectances from MODIS data is to remove cirrus contaminations in images of other channels for the study of land or ocean. The left panel of Figure 13 is a false MODIS RGB image (red: 0.66- μm ; green: 0.86- μm ; and blue: 0.55- μm channel) obtained over Victoria Island, Coronation Gulf, and Dease Strait in northern Canada at 19:15 UTC September 2, 2000. In this image, cirrus contamination is evident. The middle panel of Fig. 13 shows the cirrus image based on 1.375- μm channel measurement. After the reflectance of cirrus is retrieved using 0.66- and 1.375- μm channels, cirrus effects can be removed, as is shown in the right panel of Fig. 13. Both land and water surface features are seen more clearly in the cirrus-effect-removed image. Thus, satellite images for which the cirrus contamination has been removed can provide more accurate information about the characteristics of the earth's surfaces.

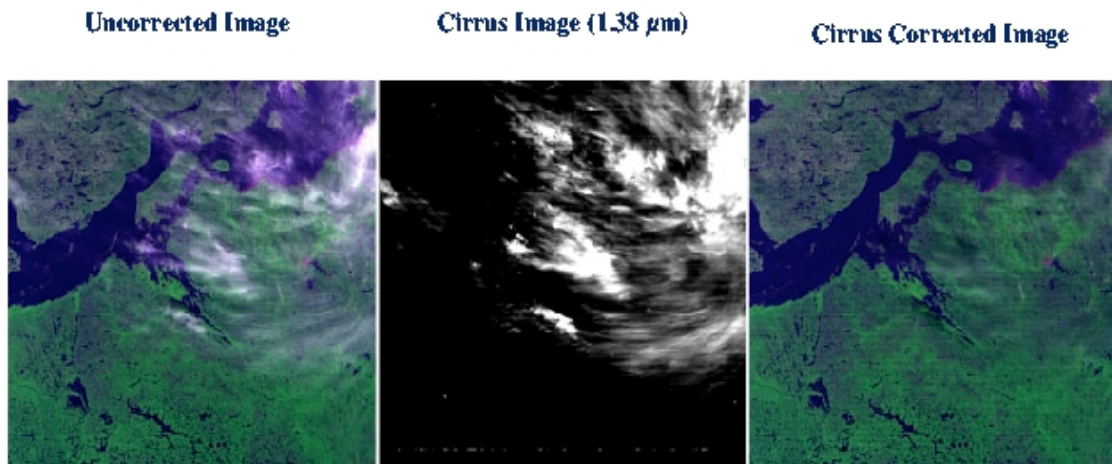


Fig. 13. An example of detecting cirrus and correcting cirrus path radiances for improved surface reflectance retrievals over northern Canada. See text for additional discussion.

3.4. Sample level 3 Monthly-Mean Global Cirrus Reflectance Images. Figure 14a shows an example of level 3 cirrus reflectance products. It is a global cirrus reflectance image of the

monthly mean for January of 2002. Two branches of cirrus clouds in the tropical Pacific Ocean regions are present. Large amounts of cirrus clouds over areas east of Japan and south of Alaska in the Pacific Ocean are seen. Figure 14b shows a global cirrus reflectance image of the monthly-mean for July of 2002. Large amounts of cirrus clouds are observed over the western part of Atlantic Ocean during the northern hemisphere summer. The overall cloud patterns in Fig. 14b are very different from those in Fig. 14a. This demonstrates that it is easy to see seasonal variations of high clouds from MODIS data.

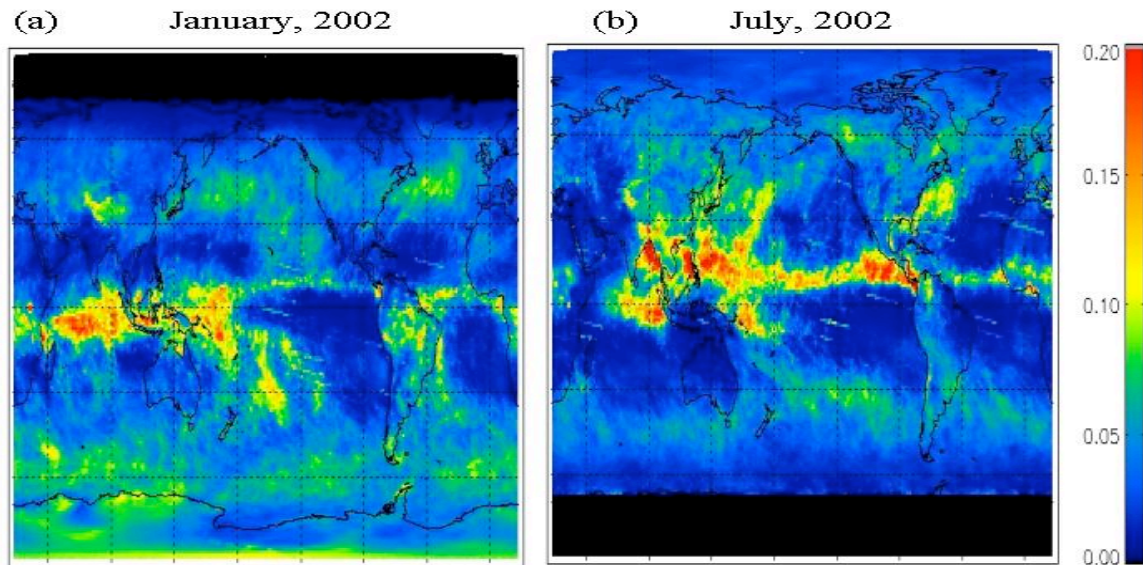


Fig. 14. Monthly-mean global cirrus reflectance images for January and July of 2002.

4. LESSONS LEARNED

The physics and atmospheric spectroscopic principles for the retrieval of water vapor amount using narrow channels near 0.94- μm and for cirrus detections using the 1.375- μm MODIS channel are well known. During the development of the MODIS near-IR water vapor algorithm and cirrus reflectance algorithm, the high spatial resolution (~ 20 m) hyperspectral imaging data collected with the NASA JPL AVIRIS instrument were used to guide and to test both algorithms. As a result, the two algorithms are fairly robust when applied to the lower spatial resolution (~ 1 km) MODIS data. We would have followed the same procedures for the development of both algorithms if we were assigned the tasks of developing both algorithms again.

In late 1992, many MODIS Science Team members supported the idea of adding the 1.38- μm channel on MODIS for cirrus detections. Unfortunately, this channel has not been widely used by members of MODIS Science Team to improve the MODIS land, ocean, and atmospheric data products. At present, many MODIS data products, such as those reported on

the most recent NASA MODIS brochure (NP-2002-1-423-GSFC) are still contaminated by the thin cirrus absorption and scattering effects.

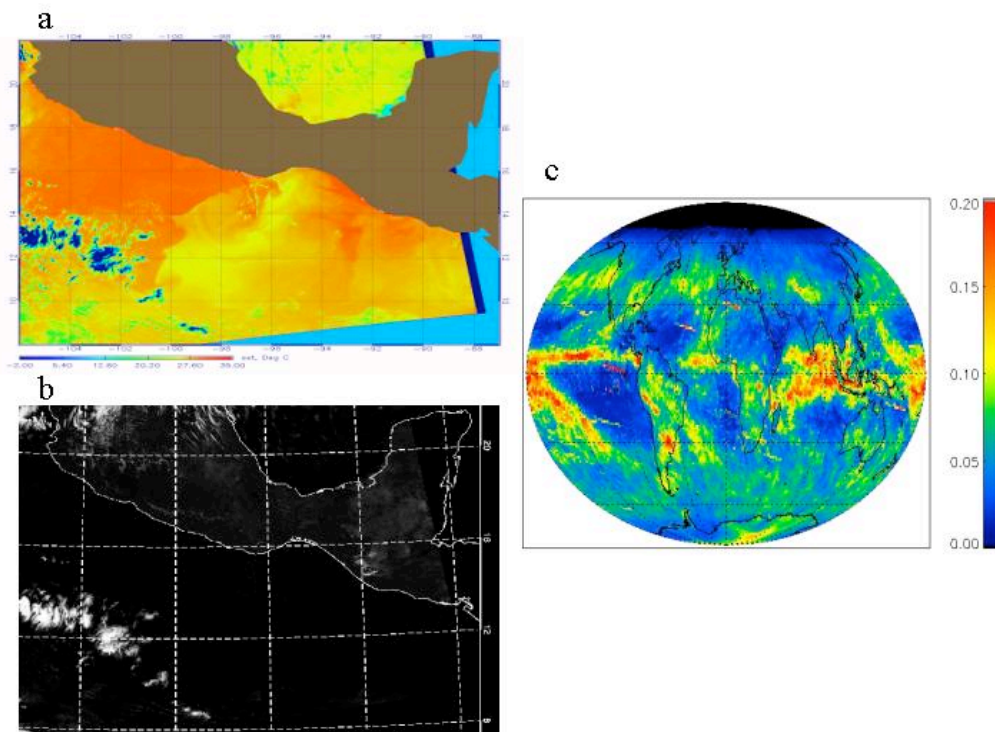


Fig. 15. (a) – a MODIS SST image over Central America; (b) – a cirrus cloud image over the same area; and (c) – a global monthly-mean cirrus image.

Cirrus clouds are widely distributed around the globe. At any given moment, more than 50% of the area is covered by cirrus clouds based on our observations with the 1.375-micron MODIS channel. We think that there are now great needs for assessing the cirrus-contamination problems for many standard MODIS data products. Here we would like to show examples of cirrus contaminations on the IR sea surface temperature data products. We show in Figure 15a an IR SST temperature image downloaded from the MODIS Ocean Group’s web site. The image was retrieved with the MODIS SST algorithm from one set of MODIS data acquired over Central America on December 3, 2002 at UTC 2000. Figure 15b shows the cirrus cloud image processed from the MODIS 1.38-micron channel data. This channel is very sensitive in detecting thin cirrus clouds. By comparing Figs. 15a and 15b, it is seen that the SST values are small (blue in Fig 15a image) over areas covered by cirrus clouds. The shapes of the white clouds in Fig. 15b are exactly the same as those blue features in Fig. 15a. This demonstrates clearly that the current MODIS SST algorithm does not properly estimate surface temperatures over areas affected by cirrus clouds. The absorption effects by ice particles in cirrus clouds were directly passed over to the Level 2 SST data products. Although cloud mask is used in the generation of Level 3 MODIS

SST data products, pixels slightly contaminated by thin cirrus clouds are inevitably used in the generation of Level 3 global SST data products. Figure 15c shows a monthly-mean cirrus reflectance image over the globe for December of 2002. These clouds are distributed unevenly at different latitudes and longitudes. Because cirrus clouds cover large portions of the earth's surface areas and because the MODIS SST algorithm does not correct for the cirrus absorption effects, the SST products retrieved from the MODIS data have variable levels of biases over large areas in different geographical regions.

The cirrus-contaminated MODIS SST data product has been used by “un-suspecting” atmospheric modelers. Scientifically unjustified conclusions have been reported during the 2003 San Francisco AGU conference, and also reported on the cover page of the 28 October 2003 issue of AGU's EOS magazine. We feel that NASA should properly inform the end users of the MODIS data products about the cirrus-contamination problems.

5. REFERENCES

- Asrar, G., R. Greenstone, (Editors), Mission to planet earth/earth observing system reference handbook, National Aeronautics and Space Administration, Goddard Space Flight Center, Mail Code 900, Greenbelt, MD 20771, USA, 277p., 1995.
- Gao, B.-C., P. Yang, W. Han, R.-R. Li, and W. J. Wiscombe, An algorithm using visible and 1.38- μm channels to retrieve cirrus cloud reflectances from aircraft and satellite data, *IEEE Trans. Geosci. Remote Sensing*, 40, 1659 – 1668, 2002.
- Gao, B.-C., M. J. Montes, Z. Ahmad, and C. O. Davis, Atmospheric correction algorithm for hyperspectral remote sensing of ocean color from space, *Appl. Opt.*, 39, 887-896, 2000.
- Gao, B.-C., Y. J. Kaufman, W. Han, and W. J. Wiscombe, Correction of thin cirrus path radiance in the 0.4 - 1.0 μm spectral region using the sensitive 1.375- μm cirrus detecting channel, *J. Geophys. Res.*, 103, 32169-32176, 1998.
- Gao, B.-C., and Y. J. Kaufman, Selection of the 1.375- μm MODIS channel for remote sensing of cirrus clouds and stratospheric aerosols from space, *J. Atm. Sci.*, 52, 4231-4237, 1995.
- Gao, B.-C., A. F. H. Goetz, and W. J. Wiscombe, Cirrus cloud detection from airborne imaging spectrometer data using the 1.38 μm water vapor band, *Geophys. Res. Lett.*, 20, 301-304, 1993.
- Gao, B.-C., and A. F. H. Goetz, Column atmospheric water vapor and vegetation liquid water retrievals from airborne imaging spectrometer data, *J. Geophys. Res.*, 95, 3549-3564, 1990.
- Green, R. O., M. L. Eastwood, C. M. Sarture, T. G. Chrien, M. Aronsson, B. J. Chippendale, J. A. Faust, B. E. Pavri, C. J. Chovit, M. S. Solis, M. R. Olah, O. Williams, Imaging

spectrometry and the airborne visible infrared imaging spectrometer (AVIRIS), *Remote Sens. Env.*, 65, 227-248, 1998.

- Kaufman, Y. J., and B.-C. Gao, Remote sensing of water vapor in the near IR from EOS/MODIS, *IEEE Trans. Geosci. Remote. Sensing*, 30, 871-884, 1992.
- King, M. D., W. P. Menzel, Y. J. Kaufman, D. Tanre, B.-C. Gao, S. Platnick, S. A. Ackerman, L. A. Remer, R. Pincus, and P. A. Hubanks, Cloud and aerosol properties, precipitable water, and profiles of temperature and water vapor from MODIS, just published by *IEEE Trans. Geosci. Remote Sensing* in March 2003.
- King, M. D., Y. J. Kaufman, W. P. Menzel, and D. Tanre, Remote sensing of cloud, aerosol and water vapor properties from the Moderate Resolution Imaging Spectrometer (MODIS), *IEEE Trans. Geosci. Remote Sens.*, 30, 2-27, 1992.
- Kneizys, F. X., E. P. Shettle, L. W. Abreu, J. H. Chetwynd, G. P. Anderson, W. O. Gallery, J. E. A. Selby, and S. A. Clough, Users guide to LOWTRAN 7, *AFGL-TR-8-0177*, Air Force Geophys. Lab., Bedford, Mass., 1988.
- Rothman, L. S., C. P. Rinsland, A. Goldman, S. T. Messie, D. P. Edwards, J. M. Flaud, A. Perri, C. Camy-Peyret, V. Dana, J. Y. Mandin, J. Schroeder, A. McCann, R. R. Gamach, R. B. Wattson, K. Yoshino, K. V. Chance, K. W. Jucks, L. R. Brown, V. Nemtchinov, and P. Varanasi, "The HITRAN molecular spectroscopic database and HAWKS (HITRAN Atmospheric Workstation): 1996 edition," *J. Quant. Spectrosc. Radiat. Transfer*, vol. 60, pp. 665-710, 1998.
- Salomonson, V. V., W. L. Barnes, P. W. Maymon, H.E. Montgomery, and H. Ostrow, MODIS: Advanced facility instrument for studies of the earth as a system, *IEEE Trans. Geosci. Remote Sens.*, 27, 145-153, 1989.
- Vane, G., R.O. Green, T.G. Chrien, H.T. Enmark, E.G. Hansen, and W.M. Porter, The Airborne Visible Infrared Imaging Spectrometer, *Remote Sens. Env.*, 44(2/3), 127-143, 1993.

6. PUBLICATIONS

With the generous financial support from NASA during the past decade, we have published a number of high quality scientific papers. Listed below are some of the papers:

- Gao, B.-C., and Y. J. Kaufman, Water vapor retrievals using Moderate Resolution Imaging Spectrometer (MODIS) near-IR channels, *J. Geophys. Res.*, 108, 4389 – 4398, 2003 (doi: 10.1029/2002JD003023).
- Gao, B.-C., P. Yang, G. Guo, S. K. Park, W. J. Wiscombe, and B.-D. Chen, Measurements of water vapor and high clouds over the Tibetan Plateau with the Terra MODIS instrument, *IEEE Trans. Geosci. Remote Sensing*, 41, 895-900, 2003 (doi: 10.1109/TGRS.2003.810704).

- Li, R.-R., Y. J. Kaufman, B.-C. Gao, and C. O. Davis, Remote sensing of suspended sediments and shallow coastal waters, *IEEE Trans. Geosci. Remote Sensing*, 41, 559-566, 2003 (doi: 10.1109/TGRS.2003.810227).
- Gao, B.-C., P. Yang, and R.-R. Li, Detection of high clouds in polar regions during the daytime using the MODIS 1.375- μ m channel, *IEEE Trans. Geosci. Remote Sens.*, 41, 474-481, 2003 (doi: 10.1109/TGRS.2002.808290).
- King, M. D., W. P. Menzel, Y. J. Kaufman, D. Tanre, B.-C. Gao, S. Platnick, S. A. Ackerman, L. A. Remer, R. Pincus, and P. A. Hubanks, Cloud and aerosol properties, precipitable water, and profiles of temperature and humidity from MODIS, *IEEE Trans. Geosci. Remote Sens.*, 41, 442-458, 2003 (doi: 10.1109/TGRS.2002.808226).
- Yang, P., H.-L. Wei, B. A. Baum, H.-L. Huang, A. J. Heymsfield, Y. X. Hu, B.-C. Gao, and D. D. Turner, The spectral signature of mixed-phase clouds composed of non-spherical ice crystals and spherical liquid droplets in the terrestrial window region, *J. Quant. Spectros. Radit. Transfer*, 79-80, 1171-1188, 2003 (doi: 10.1016/S0022-4073(02)00348-5).
- Gao, B.-C., Y. J. Kaufman, D. Tanre, and R.-R. Li, Distinguishing tropospheric aerosols from thin cirrus clouds for improved aerosol retrievals using the ratio of 1.38- μ m and 1.24- μ m channels, *Geophys. Res. Lett.*, 29, 1890, 2002 (doi: 10.1020/2002GL015475).
- Gao, B.-C., P. Yang, W. Han, R.-R. Li, and W. J. Wiscombe, An algorithm using visible and 1.38-micron channels to retrieve cirrus cloud reflectances from aircraft and satellite data, *IEEE Trans. Geosci. Remote Sensing*, 40, 1659 – 1668, 2002 (doi: 10.1109/TGRS.2002.802454).
- Yang, P., B.-C. Gao, W. J. Wiscombe, M. I. Mishchenko, S. Platnick, H.-L. Huang, B. A. Baum, Y. X. Hu, D. Winker, S.-C. Tsay, and S. K. Park, Inherent and apparent scattering properties of coated or uncoated spheres embedded in an absorbing host medium, *Appl. Opt.*, 41, 2740 – 2759, 2002.
- Yang, P., B.-C. Gao, B. A. Baum, W. Wiscombe, Y. Hu, S. L. Nasiri, P. F. Soulen, A. J. Heymsfield, G. M. McFarquhar, and L. M. Miloshevich, Sensitivity of cirrus bidirectional reflectance to vertical inhomogeneity of ice crystal habits and size distributions for two Moderate-Resolution Imaging Spectroradiometer (MODIS) bands, *J. Geophys. Res.*, 106, 17267-17291, 2001
- Yang, P., B.-C. Gao, B. A. Baum, Y. X. Hu, W. J. Wiscombe, S.-C. Tsay, D. M. Winker, Radiative properties of cirrus clouds in the infrared (8-13 micron) spectral region, *J. Quant. Spectro. Radiative Transfer*, 70, 473-504, 2001.
- Yang, P., B.-C. Gao, B. A. Baum, Y. X. Hu, W. J. Wiscombe, M. I. Mishchenko, D. M. Winker, and S. L. Nasiri, Asymptotic solutions for optical properties of large particles with strong absorption, *Appl. Opt.*, 40, 1532 – 1547, 2001.

- Gao, B.-C., and R.-R. Li, Quantitative improvement in the estimates of NDVI values from remotely sensed data by correcting thin cirrus scattering effects, *Remote Sens. Env.*, 74, 494-502, 2000.
- Kleidman, R. G., Y. J. Kaufman, L. A. Remer, R. A. Ferrare, and B.-C. Gao, Remote sensing of total precipitable water vapor in the near-IR over ocean glint, *Geophys. Res. Lett.*, 27, 2657-2660, 2000.
- Gao, B.-C., A practical method for simulating AVHRR-consistent NDVI data series using narrow MODIS channels in the 0.5 - 1.0 μm spectral range, *IEEE Transa. Geosci. Remote Sens.*, 38, 1969-1975, 2000.
- Yang, P., K. N. Liou, M. I. Mishchenko, and B.-C. Gao, Efficient finite-difference time-domain scheme for light scattering by dielectric particles: application to aerosols, *Appl. Opt.*, 39, 3727-3737, 2000.
- Gao, B.-C., M. J. Montes, Z. Ahmad, and C. O. Davis, Atmospheric correction algorithm for hyperspectral remote sensing of ocean color from space, *Appl. Opt.*, 39, 887-896, 2000.
- Gao, B.-C., Y. J. Kaufman, W. Han, and W. J. Wiscombe, Correction of thin cirrus path radiance in the 0.4 - 1.0 μm spectral region using the sensitive 1.375- μm cirrus detecting channel, *J. Geophys. Res.*, 103, 32169-32176, 1998.
- Wald, A., Y. J. Kaufman, D. Tanre, and B.-C. Gao, Daytime and nighttime detection of mineral dust over desert using infrared spectral contrast, *J. Geophys. Res.*, 103, 32307-32313, 1998.
- Gao, B.-C., W. Han, S.-C. Tsay, and N. F. Larsen, Cloud detection over arctic region using airborne imaging spectrometer data during the daytime, *J. Appl. Meteorol.*, 37, 1421-1429, 1998.
- Kaufman, Y. J., A. Wald, L. A. Remer, B.-C. Gao, R. R. Li, and L. Flynn, The MODIS 2.1- μm channel - Correlation with visible reflectance for use in remote sensing of aerosol, *IEEE Trans. Geos. Remote Sensing*, 35, 1286-1298, 1997.
- Gao, B.-C., NDWI - A normalized difference water index for remote sensing of vegetation liquid water from space, *Remote Sens. Env.*, 58, 257-266, 1996.
- Gao, B.-C., and Y. J. Kaufman, Selection of the 1.375- μm MODIS channel for remote sensing of cirrus clouds and stratospheric aerosols from space, *J. Atm. Sci.*, 52, 4231-4237, 1995.
- Gao, B.-C., and R. O. Green, Presence of terrestrial atmospheric gas absorption bands in standard extraterrestrial solar irradiance curves in the near-IR spectral region, *Appl. Opt.*, 34, 6263-6268, 1995.

- Hutchison, K. D., K. R. Hardy, and B.-C. Gao, Improved detection of optically-thin cirrus clouds in nighttime multispectral meteorological satellite imagery using total integrated water vapor information, *J. Appl. Meteorol.*, *34*, 1161-1168, 1995.
- Gao, B.-C., and W. J. Wiscombe, Surface-induced brightness temperature variations and their effects on detecting thin cirrus clouds using IR emission channels in the 8-12 μm region, *J. Appl. Meteorol.*, *33*, 568-570, 1994.
- Gao, B.-C., A. F. H. Goetz, Ed. R. Westwater, R. O. Green, and J. E. Conel, Possible near-IR channels for remote sensing precipitable water vapor from geostationary satellite platforms, *J. Appl. Meteorol.*, *32*, 1791-1801, 1993.
- Gao, B.-C., A. F. H. Goetz, and W. J. Wiscombe, Cirrus cloud detection from airborne imaging spectrometer data using the 1.38 μm water vapor band, *Geophys. Res. Lett.*, *20*, 301-304, 1993.
- Kaufman, Y. J., and B.-C. Gao, Remote sensing of water vapor in the near IR from EOS/MODIS, *IEEE Trans. Geosci. Remote Sensing*, *30*, 871-884, 1992.
- Gao, B.-C., Ed. R. Westwater, B. B. Stankov, D. Birkenheuer, and A. F. H. Goetz, Comparison of column water vapor measurements using downward-looking optical and infrared imaging systems and upward-looking microwave radiometer, *J. Appl. Meteorol.*, *31*, 1193-1201, 1992.
- Gao, B.-C., and A. F. H. Goetz, Cloud area determination from AVIRIS data using water vapor channels near 1 μm , *J. Geophys. Res.*, *96*, 2857-2864, 1991.
- Gao, B.-C., and A. F. H. Goetz, Column atmospheric water vapor and vegetation liquid water retrievals from airborne imaging spectrometer data, *J. Geophys. Res.*, *95*, 3549-3564, 1990.